Supplementary Information for

Optimal Sound-Absorbing Structures

Min Yang, Shuyu Chen, Caixing Fu, Ping Sheng

I. Causality constraint on sound absorbing structures

Consider a layer of composite material backed by a rigid reflective wall (Fig. S1a). In response to an incident sound wave, the reflected sound pressure $p_r(t)$ is the superposition of the direct reflection of the incoming sound pressure at that instant, $p_i(t)$ plus those in response to the incoming sound wave at earlier time, $p_i(t-\tau)$, with $\tau > 0$. Hence

$$p_r(t) = \int_0^\infty K(\tau) p_i(t-\tau) d\tau , \tag{S1}$$

where $K(\tau)$ is the response kernel in the time domain. By carrying out Fourier transform $p_{i/r}(\omega) = \int_{-\infty}^{\infty} p_{i/r}(t) e^{i\omega t} dt$, the reflection coefficient for each frequency may be expressed as

$$R(\omega) \equiv \frac{p_r(\omega)}{p_i(\omega)} = \int_0^\infty K(\tau) e^{i\omega\tau} d\tau . \tag{S2}$$

From Eq. (S2), $R(\omega)$ is an analytic function of complex ω in the upper half of the complex ω plane. In terms of the wavelength $\lambda = 2\pi v_0 / \omega$, where v_0 is the speed of sounds in air, that means $R(\lambda)$ has no singularities in the lower half-plane of complex λ, but may have zeros that represent total absorptions of incoming energy. Here the imaginary part of λ reflects dissipation.

To determine the constraint on the reflection coefficient $R(\lambda)$ by the causality principle, we introduce an ancillary function $\tilde{R}(\lambda)$ after Fano and Rozanov[1, 2],

$$\tilde{R}(\lambda) \equiv R(\lambda) \prod_n \frac{\lambda - \lambda_n^*}{\lambda - \lambda_n} , \tag{S3}$$

where λ_n, satisfying $R(\lambda_n) = 0$, are the zeros located in the lower half-plane of complex λ, and $*$ stands for complex conjugation. Since $\tilde{R}$ has neither zeros nor poles at $\mathrm{Im}(\lambda) < 0$, $\ln \tilde{R}$ is an analytic function in the lower half-plane of complex λ and the Cauchy theorem is valid, i.e., the integral over a closed contour C in the lower half-plane of complex λ should yield zero, where the contour consists of the real axis of and the semicircle C_∞, which belongs to the lower half-plane and has infinite radius as shown in Fig. S1b. Hence

$$\int_C \ln\tilde{R}d\lambda = \int_{-\infty}^{+\infty} \ln\tilde{R}d\lambda + \int_{C_\infty} \ln\tilde{R}d\lambda = 0. \quad \text{(S4)}$$

Note that $|\tilde{R}| = |R|$ at real wavelengths and $\ln|R|$ is an even function of λ according to its definition Eq. (S2). Taking the real part of Eq. (S4) yields

$$\mathrm{Re}\int_C \ln\tilde{R}d\lambda = 2\int_0^\infty \ln|R|d\lambda + \mathrm{Re}\int_{C_\infty} \ln R d\lambda + \mathrm{Re}\sum_n \int_{C_\infty} \ln\frac{\lambda-\lambda_n^*}{\lambda-\lambda_n}d\lambda = 0. \quad \text{(S5)}$$

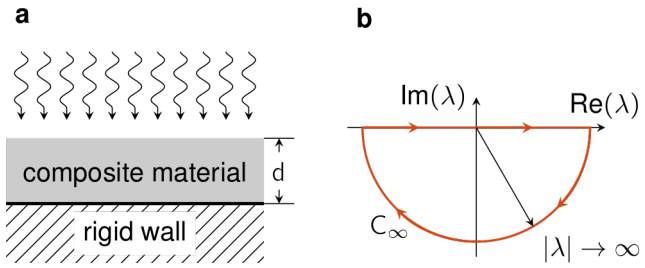

Fig. S1 (**a**) Schematic for the geometry of composite absorbing layer. (**b**) The contour for the integral in Eq. (S4).

To calculate the second integral on the right-hand-side of Eq. (S5), we consider the infinite-wavelength limit of R, i.e., the static limit. The reflection from a composite material layer can be characterized by an effective bulk modulus B_{eff} relating to its surface responses[3]. The surface displacement u under a pressure p is therefore given by the relation $(\text{pressure}) = (\text{effective bulk modulus}) \times (\text{strain})$, or $u = pd / B_{\text{eff}}$ with d being the sample thickness. The resulting surface impedance is given by $Z = ip/(\omega u) = iZ_0 B_{\text{eff}}\lambda/(2\pi B_0 d)$ with $Z_0 = B_0 / v_0$ being the air impedance and B_0 the bulk modulus of air. Therefore, the reflection coefficient $R = (Z - Z_0)/(Z + Z_0)$ is given by

$$R = \frac{1 + i2\pi dB_0/(\lambda B_{\text{eff}})}{1 - i2\pi dB_0/(\lambda B_{\text{eff}})}. \quad \text{(S6)}$$

Since $\lim_{|\lambda|\to\infty} \ln R = i4\pi dB_0/(\lambda B_{\text{eff}})$, the contour integral is therefore given by

$$\int_{C_\infty} \ln R d\lambda = \lim_{|\lambda|\to 0} \int_0^{-\pi} i\lambda \ln R d\theta = 4\pi^2 dB_0 / B_{\text{eff}}, \quad \text{(S7)}$$

where θ is the argument of complex λ. It should be noted that by taking the limit of $|\lambda| \to \infty$ in the above contour integral, one is essentially counting all the poles of $\ln R$ in the lower half of the complex λ plane, with the imaginary part of each pole being relevant to the absorption of each resonance of the system. This is evident from the fact that in our previous work[3], it has been shown that the static limit the effective bulk modulus $B_{\text{eff}}(\lambda \to \infty) = \rho_0 d^2 \left(\sum_n \alpha_n / \Omega_n\right)^{-1}$ with Ω_n being the nth resonance

frequency of the system and α_n the relevant oscillator strength defined in the main text. Hence taking the limit of $|\lambda| \to \infty$ implies all the absorptions related to the resonances of the system are taken into account. In fact, for the designed structures shown in this work, if we let $d = \bar{d}$ as defined in Eq. (S19) below, then the above formula for $B_{\text{eff}}(\lambda \to \infty)$ is accurately equal to B_0 / φ with porosity $\varphi \equiv V_{\text{air}} / V_{\text{tot}}$ being the volume fraction of the air phase. This is in agreement with Wood's formula for the composite effective bulk modulus in the static limit, given by $B_{\text{eff}}^{-1} = \varphi B_0^{-1} + (1-\varphi) B_{\text{solid}}^{-1}$. Since $B_{\text{solid}} >> B_0$, $B_{\text{eff}} = B_0 / \varphi$ follows. In addition, for samples with identical FP channels either straight or folded, $\varphi = \phi = S_{\text{air}} / S_{\text{tot}}$ where S_{air} is the area of FP channels' total surface cross sectional area and S_{tot} being the total area of the sample surface exposed to incident sound. Hence in this work we have $B_{\text{eff}} = B_0 / \phi$.

For the third integral on the right-hand-side of Eq. (S5), since $\lim_{|\lambda| \to \infty} \ln[(\lambda - \lambda_n^*) / (\lambda - \lambda_n)] = i2\text{Im}(\lambda_n) / \lambda$, we have

$$\int_{C_\infty} \ln \frac{\lambda - \lambda_n^*}{\lambda - \lambda_n} d\lambda = \lim_{|\lambda| \to \infty} \int_0^{-\pi} i\lambda \ln \frac{\lambda - \lambda_n^*}{\lambda - \lambda_n} d\theta = 2\pi \text{Im}(\lambda_n). \tag{S8}$$

Substitution of Eqs. (S7) and (S8) into Eq. (S5) yields

$$-\int_0^\infty \ln |R(\lambda)| \, d\lambda = 2\pi^2 d(B_0 / B_{\text{eff}}) + \pi \sum_n \text{Im}(\lambda_n). \tag{S9}$$

As $[1 - A(\lambda)] = |R(\lambda)|^2$, where $A(\lambda)$ stands for the absorption coefficient, and all λ_n are in the lower half-plane, i.e., $\text{Im}(\lambda_n) < 0$, we therefore have the inequality

$$d_{\min} = \frac{1}{4\pi^2} \frac{B_{\text{eff}}}{B_0} \left| \int_0^\infty \ln[1 - A(\lambda)] d\lambda \right| \le d. \tag{S10}$$

It follows from Eq. (S9) that the equality in (S10) is attained when $R(\lambda)$ has no zeros in the lower half-plane of complex λ. Such $R(\lambda)$ corresponds to the minimum phase-shift frequency dependence[1, 2] for which the variation of the phase of the reflection coefficient with λ does not exceed 2π, in the domain $0 < \lambda < \infty$.

II. Inclusion of higher order FP resonances in the design strategy

In this section we give the derivation of the design algorithm that includes all the higher order FP resonances. For a FP channel with length ℓ_n, its surface impedance is defined at its mouth, $z = 0$, by $Z = p(0) / v(0)$, with

$$p(z)=\cos\left[\omega(z+\ell_n)\sqrt{(1+i\beta/\omega)\rho_0/B_0}\right],$$

$$v(z)=-i\sin\left[\omega(z+\ell_n)\sqrt{(1+i\beta/\omega)\rho_0/B_0}\right]/Z_0.$$

For an array of N FP channels with various lengths facing the incident sound wave in parallel, their total impedance is given by

$$Z=iZ_0\left\{\phi\sum_{n=1}^{N}\tan\left[\omega\ell_n\sqrt{(1+i\beta/\omega)\rho_0/B_0}\right]\right\}^{-1}=i\frac{Z_0 d}{\omega v_0}\left[\sum_{n=1}^{N}\sum_{m=1}^{\infty}\frac{\alpha_n}{(2m-1)^2\Omega_n^2-\omega^2-i\beta\omega}\right]^{-1}, \quad \text{(S11)}$$

where ϕ is the structure's surface porosity (fraction of the total surface area occupied by the open mouths of the FP channels), $\Omega_n=\pi v_0/(2\ell_n)$ is the 1st-order FP resonance of the nth FP resonator, the terms with $m>1$ stand for higher order FP resonances, and oscillator strength $\alpha_n=2d\phi/(\ell_n N)=4d\phi\Omega_n/(\pi v_0 N)$. It is easy to see that Eq. (S11) is equivalent to Eq. (2) in the main text if we take only the terms with $m=1$.

In the ideal case, ℓ_n is continuously distributed, i.e., Ω_n is a continuous variable, Eq. (S11) can be converted into an integral:

$$\begin{aligned}Z&\simeq i\lim_{\beta\to 0}\frac{Z_0 d}{\omega v_0}\left[\int_0^{\infty}\sum_{m=1}^{\infty}\frac{\alpha(\Omega)D(\Omega)}{(2m-1)^2\Omega^2-\omega^2-i\beta\omega}d\Omega\right]^{-1}\\&=i\lim_{\beta\to 0}\frac{Z_0 d}{\omega v_0}\left[\int_0^{\infty}\frac{\sum_{m=1}^{\infty}\alpha(\tilde{\omega})D(\tilde{\omega})/(2m-1)}{\tilde{\omega}^2-\omega^2-i\omega\beta}d\tilde{\omega}\right]^{-1},\end{aligned} \quad \text{(S12)}$$

where $\tilde{\omega}=(2m-1)\Omega$, and $D(\Omega)$ is the modes density of the 1st-order FP resonances. For $\beta\to 0$, the real part of the integral in Eq. (S12) contributes negligibly, owing to the oscillatory nature of the integrant. The imaginary part of $\lim_{\beta\to 0}(\tilde{\omega}^2-\omega^2-i\beta\omega)^{-1}$ can be accurately approximated by a delta function, hence we have

$$Z(\omega)\simeq\frac{Z_0 d}{\pi\omega v_0}\left[\int_0^{\infty}\sum_{m=1}^{\infty}\frac{\alpha(\tilde{\omega})D(\tilde{\omega})}{2m-1}\delta(\omega^2-\tilde{\omega}^2)d\tilde{\omega}\right]^{-1}=\frac{2Z_0 d}{\pi v_0}\left[\sum_{m=1}^{\infty}\frac{\alpha(\Omega)D(\Omega)}{2m-1}\bigg|_{\Omega=\omega/(2m-1)}\right]^{-1}. \quad \text{(S13)}$$

If we omit the higher order FP resonances and consider only the term $m=1$, then by recalling that $D(\Omega)=\Delta n/\Delta\Omega$, we have $\Delta\Omega/\Delta n=\pi v_0\alpha(\Omega)Z(\Omega)/(2Z_0 d)$. Since $\alpha(\Omega)=4d\phi\Omega/(N\pi v_0)$, we have $\Delta\Omega/\Delta n=(2\phi\Omega/N)[Z(\Omega)/Z_0]$. By letting $\Delta n/N\to d\bar{n}$ in the limit of $N\to\infty$, where $\bar{n}=(n-1)/N$, we have thus derived Eq. (4) in the main text.

To include the higher order FP resonances, we recognize that the additional impedances that arise from the higher order resonances are in parallel to that arising from the 1st order FP resonances. Since now we have to deal with multiple impedances even from a single FP resonator, we would like to denote that impedance related to the 1st order FP resonance to be $\tilde{Z}(\Omega)$. In that case

$$\frac{d\Omega}{dn} = \frac{\pi v_0}{2d}\left[\frac{\tilde{Z}(\Omega)}{Z_0}\right]\alpha(\Omega). \tag{S14}$$

Substitution of Eq. (S14) into Eq. (S13) and separating out the term m=1 from the m-summation, yields an equation for $\tilde{Z}(\Omega)$,

$$\tilde{Z}(\omega)^{-1} = Z(\omega)^{-1} - \sum_{m=2}^{\infty} \frac{\tilde{Z}(\Omega)^{-1}}{2m-1}\bigg|_{\Omega=\omega/(2m-1)}. \tag{S15}$$

The value of $\tilde{Z}$ can be obtained from Eq. (S15) through iterations, based on a given target impedance Z. Simultaneously, Eq. (S15) also expresses the fact that the target impedance at frequency ω is now the consequence of impedance from the 1st order FP resonance, plus the impedance from all the higher order FP resonances, added in parallel.

For example, if the target $Z = Z_0$ for $\omega > \Omega_c$ and divergent for $\omega < \Omega_c$, then the value of $\tilde{Z}$ can be determined in a piecewise fashion as follows. The piecewise fashion of the result is a natural consequence (upon iteration) of the step-function nature of the target impedance. The iteration results show that $Z_0 / \tilde{Z}_1 = 1$ in the first frequency range $\Omega \in [\Omega_c, 3\Omega_c]$, $Z_0 / \tilde{Z}_2 = 2/3$ in the second frequency range $\Omega \in [3\Omega_c, 5\Omega_c]$, $Z_0 / \tilde{Z}_3 = 7/15$ in the third frequency range $\Omega \in [5\Omega_c, 7\Omega_c]$, $Z_0 / \tilde{Z}_4 = 34/105$ in the fourth frequency range $\Omega \in [7\Omega_c, 9\Omega_c]$, $Z_0 / \tilde{Z}_5 = 269/1155$ in the fifth frequency range $\Omega \in [9\Omega_c, 11\Omega_c]$, etc. In each frequency interval i, i.e., for $\Omega \in [(2i-1)\Omega_c, (2i+1)\Omega_c]$, the 1st-order FP resonance frequency distribution can be determined by Eq. (14). That is, with the initial condition $\Omega = (2i-1)\Omega_c$ when the continuous variable $\bar{n} = (n-1)/N = \bar{n}_i = N_i / N$, where N_i denotes the total number of 1st-order FP resonances below $(2i-1)\Omega_c$, Eq. (S14) gives $\Omega_n = (2i-1)\Omega_c \exp[2\phi(\bar{n} - \bar{n}_i)\tilde{Z}_i / Z_0]$. From such 1st order FP resonance frequencies one can easily determine the required lengths of the FP resonators in the design.

In Fig. S2a we plot the natural logarithm of Ω_n as a function of $(n-1)/N$. Here the value of ϕ, needed for the evaluation of Ω_n, is taken to be the causally optimal value determined below. The function $\ln\Omega_n$ versus $(n-1)/N$ is seen to be piecewise hyper-linear. By using this result, discretization of the resonators in the actual design can be easily determined by locating the frequencies

on the vertical axis with the associated (equally-spaced) values of $(n-1)/N$ with N being the total number of FP channels one wants to use. For the broadband absorber presented in the main text with $N=16$, these frequencies are explicitly indicated by the red dotted lines in Fig. S2a.

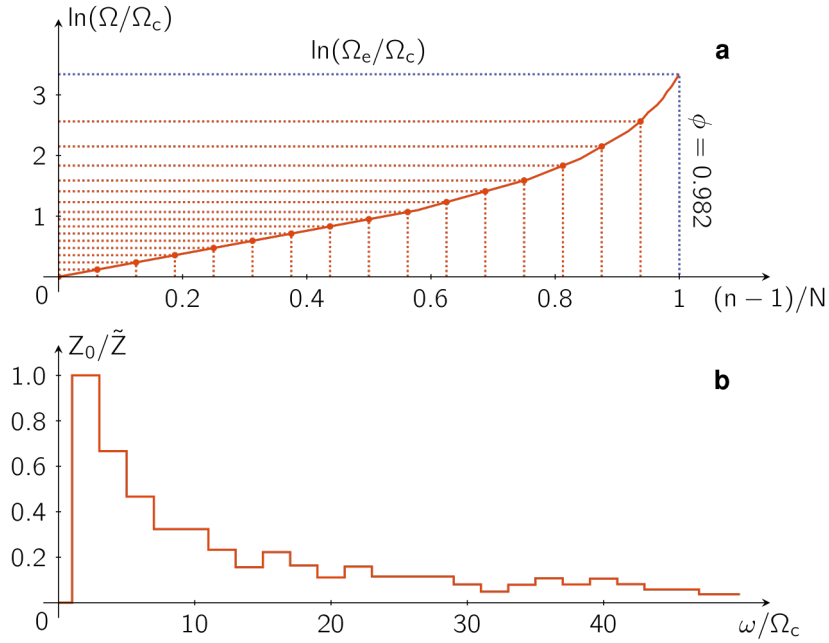

Fig. S2 (**a**) Natural logarithm of the 1st order FP resonance frequency plotted as a function of the variable $(n-1)/N$ as defined in the text. The discretized frequencies are picked off from the curve with equally-spaced intervals on the horizontal axis. They are indicated by the red dotted lines. (**b**) The iterated target impedance $\tilde{Z}$ in Eq. (S14) for the 1st-order FP resonances in the broadband absorber design, in which the contributions of higher order FP modes for each channel are taken into account. Here $\tilde{Z}$ is obtained from iterations through Eq. (S15) based on a target impedance that is equals to Z_0 above a cutoff frequency Ω_c and $Z_0/Z=0$ below the cutoff. The fast decay of $Z_0/\tilde{Z}$ (to zero) guarantees that $Z=Z_0$ can be automatically satisfied by the higher order FP modes if the channels are designed in accordance to the recipe.

One important feature for the sequence $Z_0/\tilde{Z}_i$ is that it decays to zero very quickly (Fig. S2b), i.e., the required 1st-order FP modes density in the high frequency regime is very low. This fact is relevant to the high frequency absorption behavior for the broadband absorber presented in the main text. That is, since $\sum_{m=1}^{\infty}\alpha(\Omega)D(\Omega)/(2m-1)|_{\Omega=\omega/(2m-1)}=2d/(\pi v_0)$ (this can be easily deduced from Eqs. (S13), (S14), and (S15)), Eq. (S12) can be integrated to yield

$$\frac{Z}{Z_0}=\frac{\pi}{\pi-2i\tanh^{-1}(\Omega_c/\omega)}. \tag{S16}$$

And the relevant reflection coefficient $R=(Z-Z_0)/(Z+Z_0)$ is given by

$$R=\frac{\tanh^{-1}(\Omega_c/\omega)}{\pi-i\tanh^{-1}(\Omega_c/\omega)}. \tag{S17}$$

That is, at high frequencies the reflection is zero, i.e., the absorption coefficient must approach 1. Therefore, in the broadband absorber design one can use a relatively small number of FP channels, designed for the low frequencies by following the proposed recipe above, and high absorption in the high frequencies regime becomes guaranteed. In particular, this would ensure high absorption above 5000 Hz for the broadband absorber presented in the main text, where there are no measured data.

So far, the parameter ϕ remains un-determined. Below we show that its value should not be arbitrary. Instead, it serves as the critical link between the designed mode density, the sample thickness, and the causal constraint.

In the broadband absorber, the channel length of the FP resonator is given by

$$\ell_n = \frac{\pi v_0}{2\Omega_n} = \pi v_0 \frac{\exp[2\phi(\overline{n}_i - \overline{n})\tilde{Z}_i / Z_0]}{2(2i-1)\Omega_c}, \tag{S18}$$

provided its 1st-order resonance is located in the frequency range $\Omega \in [(2i-1)\Omega_c, (2i+1)\Omega_c]$. Since the channel length can vary, we wish to know the minimum thickness of the sample by optimally folding the FP channels, without changing the overall area exposed to the incident wave. This minimum thickness $\overline{d}$ can be obtained through volume conservation of the FP channels. Here we evaluate $\overline{d}$ by focusing on only the air channels of the FP resonators. Since the FP channels' cross sections occupy a fraction ϕ of the surface area, $\overline{d}$ is given by

$$\overline{d} = \lim_{N\to\infty} \sum_{n=1}^{N} \frac{\ell_n}{N} = \pi v_0 \lim_{N\to\infty} \int_{\Omega_c}^{\Omega_e(\phi)} \frac{1}{\Omega} \frac{dn}{d\Omega} d\Omega \Big/ (2N), \tag{S19}$$

where the upper limit of the integral, $\Omega_e(\phi) = \lim_{N\to\infty} \Omega(n = N, \phi)$, is determined by the total number of 1st order mode number *N*, which is equal to the FP channel number. The numerical evaluation of Eq. (S19), with *N*=16, gives $\overline{d} = [0.6395 - 859.74\exp(-12.82\phi)]v_0 / (\phi\Omega_c)$. By requiring $\overline{d} = d_{\min} = 2v_0 / (\phi\Omega_c\pi)$ given in the main text, we obtain the causally optimal value $\phi_{optimal} = 0.982$, with the upper limit $\Omega_e = 28.4\Omega_c$ (indicated in Fig. S2a by the blue dotted line). Since in experimental implementation the value of ϕ is determined by the wall thickness in our design, such a high value of $\phi_{optimal}$ is not realizable in practice. However, a lower value of the actual ϕ is seen to only degrade the absorption somewhat, as long as the mode distribution (and hence the length of the channels) is designed in accordance with the ideal value $\phi_{optimal}$. The degradation effect can be seen in Fig. S6, where the designed sample has a lower surface coverage $\phi = 0.8$, leading to a degradation of reflection from its ideal value by about 5 dB, even though the actual value of the absorption coefficient is still in the range of 97-99%.

As another example, other than the broadband absorber presented in the main text, we have also considered a target absorption spectrum which starts with near-perfect absorption from 345 Hz and has a notch in the frequency interval [562 Hz, 995 Hz] where the absorption is close to zero. The target impedance is given by $Z(\omega) = Z_0[2 - A(\omega) + 2\sqrt{1 - A(\omega)}]/A(\omega)$. Based on this target impedance the impedance $\tilde{Z}(\omega)$ can be obtained from Eq. (S15) through iterations. Substitution of $\tilde{Z}$ into Eq. (S14) gives the designed resonance frequencies $\mathbf{\Omega}_n(N,\phi)$ as a function of total channel number N and the parameter ϕ. The associated FP channel length ℓ_n can then be determined. The minimum thickness of the absorber, $d_{\min} = 8.73$ cm, is determined from the casual integral (S10) of the absorption spectrum shown by the dashed line in Fig. 3c in the main text, which is based on the integral of Eq. (S12) with $N \to \infty$. In this case the value $\phi_{optimal} = 0.81$ is determined from $d_{\min} = \bar{d} = \lim_{N\to\infty} \sum_{n=1}^{N} \ell_n / N$. The experimentally measured absorption for this design, with $N = 16$, is presented in the main text as Fig. 3c. Here $\bar{d} = 8.85$ cm, and the real sample thickness is 9.03 cm due to the non-ideal folding of the channels. The result shown in Fig. 3c in the main text has a 3-mm layer of sponge placed in front; hence the total thickness of the sample is 9.33 cm.

III. Derivation of self-energy due to cross-channel coupling by evanescent waves

Since the surface impedance of the metamaterial unit is laterally inhomogeneous, it follows that the sound pressure field $p(\mathbf{x})$, where $\mathbf{x}$ denotes the lateral coordinate at the plane $z = 0$, must necessarily be inhomogeneous as well. By decomposing the pressure field as $p(\mathbf{x}) = \bar{p} + \delta p(\mathbf{x})$, where $\bar{p}$ is the surface-averaged value, it has been shown in the main text that $\delta p(\mathbf{x})$ is only coupled to the evanescent waves that decay exponential away from $z = 0$. In contrast, $\bar{p}$ couples to the far-field propagating modes. Therefore, the measured surface impedance should be given by $Z = \bar{p}/\bar{v}$ with $\bar{v} = d\bar{u}/dt$ being the surface-averaged z component of the air displacement velocity. Reflection coefficient is given by $R = (Z - Z_0)/(Z + Z_0)$.

We expand $\delta p(\mathbf{x})$ in terms of the normalized Fourier basis function $f_{\boldsymbol{\alpha}}(\mathbf{x}) = \exp[i\mathbf{k}_{\boldsymbol{\alpha}} \bullet \mathbf{x}]/L$, where $\boldsymbol{\alpha} = (\alpha_x, \alpha_y)$ is discretized by the condition that the area integral of $f_{\boldsymbol{\alpha}}$ over the surface of the metamaterial unit must vanish, due to the fact that the same condition applies to $\delta p(\mathbf{x})$. That means $|\mathbf{k}_{\boldsymbol{\alpha}}| = (2\pi/L)\sqrt{\alpha_x^2 + \alpha_y^2}$, with $\alpha_x, \alpha_y = \pm 1, \pm 2, \cdots$:

$$\delta p(\mathbf{x}, z) = \sum_{\boldsymbol{\alpha}} \delta p_{\boldsymbol{\alpha}} f_{\boldsymbol{\alpha}}(\mathbf{x}) e^{-\sqrt{k_{\boldsymbol{\alpha}}^2 - k_0^2} z}, \tag{S20}$$

where $\delta p_{\boldsymbol{\alpha}}$ denotes the expansion coefficient, and $k_0 = 2\pi/\lambda$. The exponential variation of $\delta p(\mathbf{x},z)$ means that it can couple to the z component of the air displacement velocity through Newton's law, $\partial \delta p / \partial z = -i\omega\rho_0 \delta v$, so that

$$\delta v(\mathbf{x}) = \delta v(\mathbf{x}, z=0) = \frac{-i}{\omega\rho_0} \sum_{\boldsymbol{\alpha}} \delta p_{\boldsymbol{\alpha}} \sqrt{|\mathbf{k}_{\boldsymbol{\alpha}}|^2 - k_0^2}\, f_{\boldsymbol{\alpha}}(\mathbf{x}). \tag{S21}$$

By multiplying both sides of Eq. (S21) by $f^*_{\boldsymbol{\alpha}'}(\mathbf{x})$ and integrating over the surface of the metamaterial unit's surface, we can solve for $\delta p_{\boldsymbol{\alpha}}$:

$$\delta p_{\boldsymbol{\alpha}} = i\omega\rho_0 \frac{\int_{surface} v(\mathbf{x}) f^*_{\boldsymbol{\alpha}}(\mathbf{x})\, d\mathbf{x}}{\sqrt{|\mathbf{k}_{\boldsymbol{\alpha}}|^2 - k_0^2}}, \tag{S22}$$

where $v(\mathbf{x}) = \bar{v} + \delta v(\mathbf{x})$. It should be noted that in the above, the integral of $v(\mathbf{x}) f^*_{\boldsymbol{\alpha}}(\mathbf{x})$ is the same as the integral of $\delta v(\mathbf{x}) f^*_{\boldsymbol{\alpha}}(\mathbf{x})$, since the integral of $\bar{v} f_{\boldsymbol{\alpha}}(\mathbf{x})$ is zero. By substituting Eq. (S22) into Eq. (S20) and then interchanging the order of summation and integration, we obtain

$$\delta p(\mathbf{x}) = \delta p(\mathbf{x}, z=0) = i\omega\rho_0 \int_{surface} \Lambda(\mathbf{x},\mathbf{x}') v(\mathbf{x}')\, d\mathbf{x}', \tag{S23}$$

where $\Lambda(\mathbf{x},\mathbf{x}') \equiv \sum_{\alpha} f^*_{\boldsymbol{\alpha}}(\mathbf{x}') f_{\boldsymbol{\alpha}}(\mathbf{x}) / \sqrt{|\mathbf{k}_{\boldsymbol{\alpha}}|^2 - k_0^2}$. Since $|\mathbf{k}_{\boldsymbol{\alpha}}| \gg k_0$, we can approximate $\sqrt{|\mathbf{k}_{\boldsymbol{\alpha}}|^2 - k_0^2}$ by $|\mathbf{k}_{\boldsymbol{\alpha}}|$. By discretizing the 2D coordinate $\mathbf{x}$ by its 16 values, $\mathbf{x}_n$, that denotes the center position of the nth FP channel, and replacing $d\mathbf{x}'$ by $L^2/16$ and the integral by summation, we have:

$$\delta p_n = i\omega\rho_0 \sum_{m=1}^{16} \Lambda_{nm} v_m, \tag{S24}$$

$$\Lambda_{nm} = \frac{16}{L^2} \frac{\int_{\sigma_n} f_{\boldsymbol{\alpha}}(\mathbf{x}) d\mathbf{x} \int_{\sigma_m} f^*_{\boldsymbol{\alpha}}(\mathbf{x}') d\mathbf{x}'}{|\mathbf{k}_{\boldsymbol{\alpha}}|}$$

$$= 16 \sum_{\boldsymbol{\alpha}} \frac{\sin^2(\alpha_x \pi/4) \sin^2(\alpha_y \pi/4)}{\pi^4 \alpha_x^2 \alpha_y^2 |\mathbf{k}_{\boldsymbol{\alpha}}|} \exp\left[i\mathbf{k}_{\boldsymbol{\alpha}} \bullet (\mathbf{x}_m - \mathbf{x}_n) \right], \tag{S25}$$

where σ_n denotes the cross-sectional area of the n^{th} FP channel, and $v_m = v(\mathbf{x}_m)$, $\delta p_n = \delta p(\mathbf{x}_n)$.

According to the definition of Green function, at the mouth of the n th FP channel, we have

$$v_n = -i\omega g_n (\bar{p} + \delta p_n). \tag{S26}$$

Substitution of Eq. (S24) into Eq. (S26) gives

$$v_n = -i\omega\left(g_n + \omega^2\rho_0 \sum_m g_n \Lambda_{nm} g_m + \cdots \right)\bar{p}$$

$$= -i\omega\left[\left(g_n + \omega^2\rho_0 g_n^2 \Lambda_{nn} + \omega^4 \rho_0^2 g_n^3 \Lambda_{nn}^2 + \cdots \right) + \omega^2\rho_0 \sum_{m\neq n} g_n \Lambda_{nm} g_m + \cdots \right]\bar{p}$$

$$= -i\omega\left(\frac{g_n}{1-\omega^2\rho_0 g_n \Lambda_{nn}} + \sum_m \Pi_{nm} \right)\bar{p}\,. \qquad \text{(S27)}$$

We have rearranged the series by separating the terms involving only Λ_{nn}, since $\Lambda_{nn} >> \Lambda_{nm}(m \neq n)$ by orders of magnitude. Numerically, the last term in the bracket is also small and hence only constitutes small adjustment to the results. According to the Eq. (8) in the main text, the renormalized impedance is given by $Z^{(e)} = 16\,\bar{p} \Big/ \sum_{n=1}^{16} v_n$. Substitution of Eq. (S27) (with the $\sum_m \Pi_{nm}$ term neglected) into this expression for $Z^{(e)}$ gives

$$Z^{(e)} = i\left(\frac{\omega}{16} \sum_{n=1}^{16} g_n^{(e)} \right)^{-1}, \qquad \text{(S28)}$$

where the effective Green function can be expressed in the form of the Dyson equation with a self-energy term:

$$\left(g_n^{(e)} \right)^{-1} = g_n^{-1} - \omega^2\rho_0 \Lambda\,. \qquad \text{(S29)}$$

Here $\Lambda \equiv \Lambda_{nn}$. Below we show this self-energy can predict the resonance frequency shifts of the FP resonators.

IV. Shift of the resonance frequencies due to the renormalization effect by evanescent waves

The exact Green function for a single FP channel with length ℓ_n, $g = i/(\omega Z)$, can be derived from Eq. (S11) as

$$g_n = \frac{\phi}{\omega Z_0} \tan\left[\omega \ell_n \sqrt{(1 + i\beta/\omega)\rho_0 / B_0} \right]. \qquad \text{(S30)}$$

Here the coefficient $\beta = 14.2$ Hz is an effective parameter characterizing air's viscosity in FP channels. Its value is obtained by fitting the experimental data.

The renormalized impedance $Z^{(e)}$ of the FP resonators array can then be obtained by substituting Eq. (S30) into Eqs. (S27) and (S28). Since the resonance modes are best detected by the imaginary part of the Green function, which in the present case is given by $\mathrm{Im}(G) = \mathrm{Im}\left[i \Big/ \left(\omega Z^{(e)} \right) \right]$, we have plotted the dimensionless quantity $\mathrm{Im}(G)\Omega_c Z_0$ in Fig. S3. Here $\Omega_c = 2\pi \times 345$ Hz is the cutoff frequency.

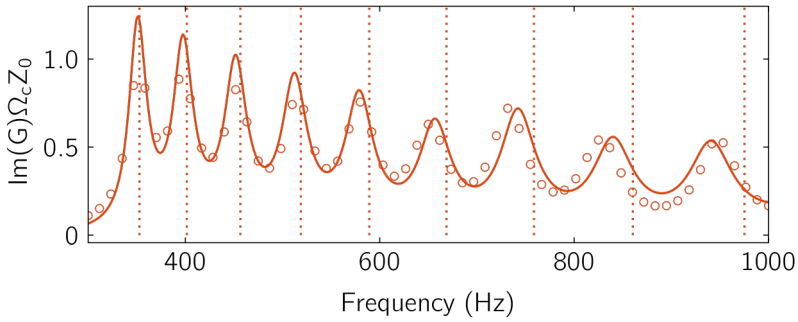

Fig. S3 The imaginary part of the Green function for the metamaterial unit, plotted as a function of frequency. The metamaterial unit consists of 16 FP channels in a 4×4 square lattice, shown in Fig. 2a of the main text. Here the solid curve is the prediction from the theory including the evanescent waves and the viscosity of air. The open circles are results deduced from experimental reflection measurements, where we have used the formula $\mathrm{Im}(G)\Omega_c Z_0 = \mathrm{Im}\left\{-i\Omega_c(R-1)/[\omega(R+1)]\right\}$. It is seen that the peak positions, which indicate the renormalized resonances, are all down-shifted from the dotted lines that mark the original FP resonance frequencies (Ω_n's). Excellent theory-experiment agreement is seen.

As shown in Fig. S3, for the metamaterial unit the theoretically predicted positions of the newly emerged resonances (solid curve) fit the experiment (open circles) very well, and they all have a clear downward shift from the original FP resonances, $\Omega_n = \pi v_0/(2\ell_n)$, denoted by the vertical dotted lines. Physically, the downshift can be understood as due to the extra air mass participating in the resonant motion at the mouth of the FP channel, arising from the evanescent waves.

V. Critical dissipation for casual optimality

In the main text, the causal optimality of the 16-units broadband absorber is achieved by placing a layer of 3 mm acoustic sponge in front of it. Here we discuss the property requirement for the sponge. The description of sponge's properties $\rho_{\mathrm{eff}} = \rho_0[1.4 + i(1420\ \mathrm{Hz})/\omega]$ is a simplified form for the effective medium theory of porous medium that assumes the solid skeleton of sponge to be rigid while sounds propagates in the pores. Adapted from Ref [5], according to the model of Johnson et al.[6], $\rho_{\mathrm{eff}} = \rho_0\alpha(\omega)$ with $\alpha(\omega)$ being the dynamic tortuosity, given by

$$\alpha(\omega) = \alpha_\infty + \frac{i\eta_0\varphi}{\omega\rho_0\kappa_0}\sqrt{1-\frac{i\omega\rho_0}{\eta_0}\left(\frac{2\alpha_\infty\kappa_0}{\Lambda_v\varphi}\right)^2}. \tag{S31}$$

Here, α_∞ is the tortuosity of a porous medium that is 1.4 in our case, η_0 is the viscosity of air, φ is the sponge porosity, and κ_0 is its static permeability. $\Lambda_v = 2\int_{V_f} v_{\mathrm{inviscid}}^2 dV / \int_{S_f} v_{\mathrm{inviscid}}^2 dS$ is the viscous characteristic length with v_{inviscid} being the air velocity field in the absence of viscosity, and the two integrals are carried on the volume of pores and the surface of solid skeleton, separately. If the

frequency is not very high, $\alpha(\omega)$ can be approximated by $\alpha_\infty + i\beta/\omega$ with $\beta = \eta_0\phi/(\rho_0\kappa_0)$. And the dissipation property for a sponge is sensitive to the ratio between its porosity and static permeability.

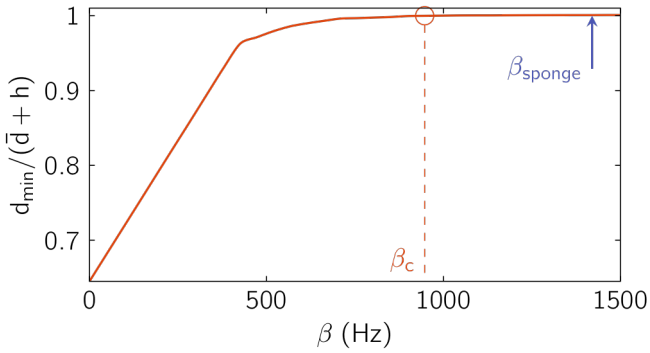

Fig. S4 The minimum thickness $d_{\min}$ of the broadband absorber in the main text, with $h = 3$ mm sponge in front, as dictated by the casual integral, Eq. (S10), in which the absorption spectrum is that predicted by the renormalized impedance $Z^{(e)}$ in Eqs. (S27) and (S28) with ρ_0 replaced by ρ_{spong}. Here the dissipation coefficient β for the front sponge has been treated as a variable. It is seen that there is a critical value $\beta_c = 946$ Hz above which the causal optimality (defined as $d_{\min} = d$) is attained. The blue arrow denotes the dissipation of the sponge used in the experiment.

In order for the addition of 3 mm sponge to the acoustic metamaterial unit to achieve causal optimality, we have calculated the casual integral, Eq. (S10), for absorption spectra with different sponge cover characterized by different values of β. The results are shown in Fig. S4, where the vertical axis is the ratio of $d_{\min}$ divided by the total thickness of the sample. Here h=3 mm is the sponge thickness, and $\bar{d}$ is the minimum thickness of the cuboid sample achievable by perfect folding of the longer FP channels. The value of $d_{\min}/(\bar{d}+h) = 1$indicates causal optimality. In Fig. S4 this ratio, with $d_{\min}$ calculated by Eq. (S10), is plotted as a function of β. It is seen that there is the existence of a critical $\beta_c = 946$ Hz. For those sponges with $\beta < \beta_c$, casual optimality cannot be satisfied. However, the acoustic sponge used in our sample is safely in the range of $\beta > \beta_c$.

VI. **Comparison with conventional acoustic materials**

In this section, we compare our metamaterial absorber with the conventional acoustic absorption materials, the micro-perforated panel (MPP) absorber and acoustic sponge. Owing to measurement accuracy, we choose to compare our 6-cm absorption structure with similar thickness MPP absorber and acoustic sponge.

The MPP absorber[4] and acoustic sponge are two very effective sound absorbers. However, the MPP has proven to be excellent only at multiple distinct frequencies, and such an absorption spectrum

can also achieve causal optimality, provided the MPP's perforated hole diameter is small enough (see Fig. S5b).

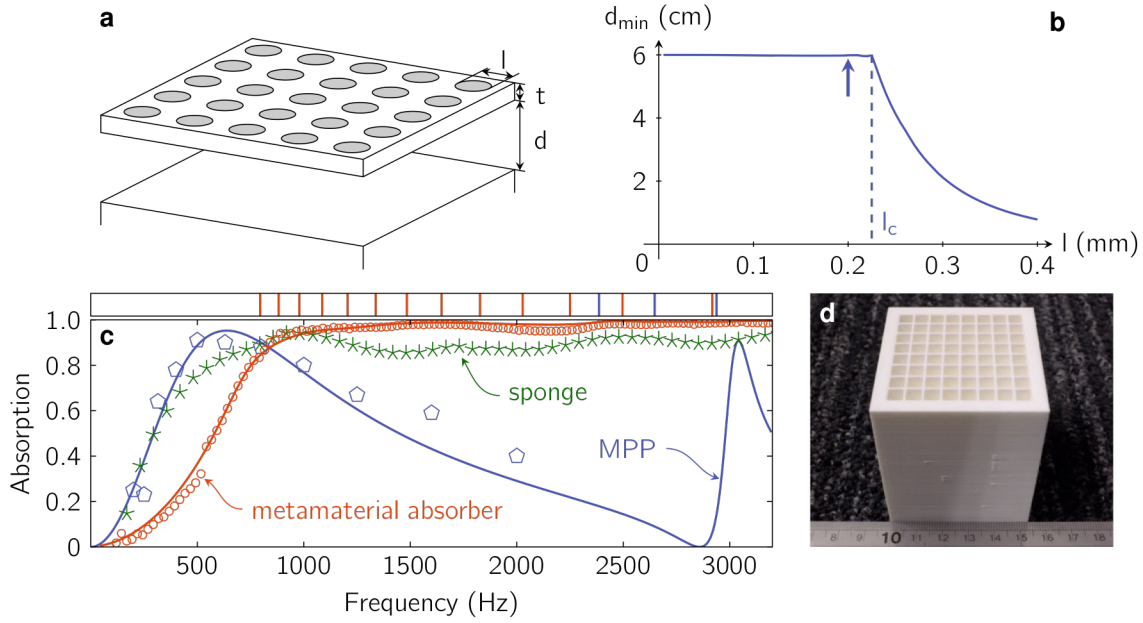

Fig. S5 (**a**) A schematic drawing for the MPP absorber. (**b**) The minimal thickness d_{min} determined by the causal integral of the absorption spectrum, Eq. (S10), for a MPP with perforation diameter l, panel thickness $t = 0.2$ mm, lattice constant $b = 2.5$ mm, and back chamber depth $d = 6$ cm. The blue arrow indicates the perforation's diameter of l =0.2 mm, whose relevant absorption spectrum (blue line and symbols) is shown in (**c**). (**c**) Comparison of the absorption spectra for the MPP (blue line (theory) and symbols (experiment)) with $l = 0.2$ mm and a total thickness of ~6 cm; the broadband metamaterial unit covered by a 3-mm layer of acoustic sponge, with a total thickness of 5.93 cm (red line (theory) and symbols (experiment)), and a layer of 6 cm-thick acoustic sponge (green symbols (measured data)). The blue curve is from Maa's theoretical model Eq. (S32), and the pentagons are the experimental data from Maa's original paper *(4)*. (**d**) A photo image of the metamaterial unit with a thickness of 5.63 cm. With the addition of 3 mm of acoustic sponge in front, the absorber has a total thickness similar to the MPP.

As shown in Fig. S5a, consider a panel that is $t = 0.2$ mm thick, with perforated holes that are arranged in a square lattice with a lattice constant $b = 2.5$ mm. The panel is backed by a chamber with $d = 6$ cm[4]. Maa's theoretical model[4] has proven to be very accurate for characterizing MPP's absorption. For uniform circular perforations with diameter l the absorption is given by[4]

$$A(\omega) = \frac{4r}{(1+r)^2 + [\omega m - \cot(\omega d / v_0)^2]}. \tag{S32}$$

Here,

$$r = \frac{32\eta_0 t}{\sigma \rho_0 v_0 l^2} k_r, \quad k_r = \left[1 + \frac{k^2}{32}\right]^{1/2} + \frac{\sqrt{2}}{32} k \frac{l}{t},$$

$$m = \frac{t}{\sigma v_0} k_m, \quad k_m = 1 + \left[1 + \frac{k^2}{2}\right]^{-1/2} + 0.85 \frac{l}{t},$$

and

$$k = l\sqrt{\omega\rho_0/(4\eta_0)}, \quad \sigma = l^2\pi/(4b^2),$$

where the quantity $\sqrt{\eta_0/(\omega\rho_0)}$ is usually denoted the viscous boundary layer thickness. Here η_0 is related to the effective air dissipation parameter β in the main text, through the solution of the sound wave propagation in the FP channel.

In Fig. S5c, the solid blue line is the theory prediction of the MPP absorption with the parameter values given above, and $l = 0.2$ mm. The open circles are the experimental results[4]. The causal integral, Eq. (S10), gives $d_{\min} \simeq d = 6$ cm, i.e., causal optimality is satisfied. In Fig. S5b, we plot the $d_{\min}$ calculated from the predicted absorption spectra. It turns out that a critical perforation diameter $l_c \simeq 0.025$ mm exists, and for $l > l_c$ causal optimality is not satisfied. It is somewhat surprising that the critical value of the perforation hole diameter agrees so well with the "best" diameter of the holes as determined from an entirely different perspective[4].

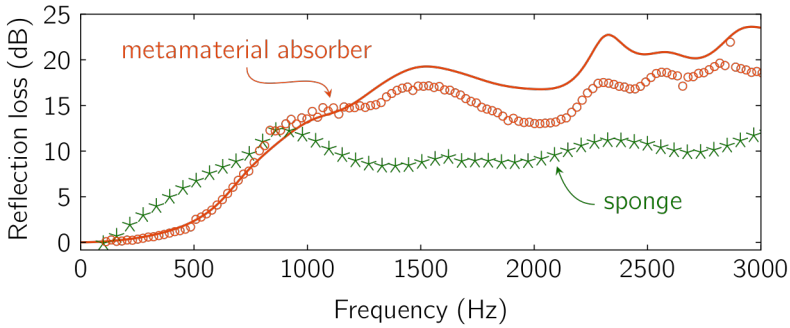

Fig. S6 Reflection loss (dB) comparison for the 6 cm thick acoustic sponge and 5.93 cm thick metamaterial absorber shown in Fig. S5c. The red curve represents the theory prediction of our metamaterial absorber, and the open circles are from experiment. The poorer experimental absorption can be attributed to the lower achievable value of $\phi = 0.8$ as compared to its optimal value $\phi_{optimal}$. Its effect can be easily assessed by the formula $A = 1 - \left[(Z/Z_0 - 1)/(Z/Z_0 + 1)\right]^2$. If Z/Z_0 is 20% larger than $Z/Z_0 = 1$, i.e., $Z/Z_0 \cong 1.2$ as expected by the lower value of $\phi = 0.8$, then the absorption would be lowered by 0.8%. The green stars are the experimentally measured data of acoustic sponge. To reach the absorption level of our design structure within the target range, the sponge thickness would need to be increased by at least 50%. If thin walls can be realized technically so that the theory prediction can be realized, then the advantage of the metamaterial absorber in the target frequency range (solid line) is seen to be quite substantial.

To compare with the particular MPP absorber whose absorption spectrum is shown in Fig. S5c, we have redesigned our broadband metamaterial absorber by setting the cutoff frequency $\Omega_c = 650$ Hz, and folded the 16 FP channels into a 5.63 cm thick cuboid. The value of $\phi = 0.8$ for the sample is the same as that for the broadband absorber presented in the main text, even though the FP channels were designed with $\phi_{optimal} = 0.982$. A photo image of the sample is shown in Fig. S5d. Four of such units

were arranged into a square with the cross section that fits the cross section of the impedance tube (see Fig. S5d). The metamaterial unit was covered by a layer of 3 mm thick acoustic sponge, so that the total thickness of the absorber, 5.93 cm, is similar to that of the MPP in Maa's work[4]. The absorption spectrum of this metamaterial absorber is shown in Fig. S5c (red symbols for the experiment, red line the theory prediction). It is seen that near-perfect flat absorption starts around 752 Hz. The causal integral of this spectrum gives $d_{\min} = 5.86$ cm, very close to the actual thickness of the sample. In the same figure, we also compared the absorption of a layer of 6 cm sponge with rigid substrate. The sponge absorption coefficient is noted to be also causally optimal. It is clear that the three causally optimal structures exhibit absorption behaviors that are very different. The MPP starts its maximum absorption at a lower frequency, ~ 640 Hz, but quickly drops to nearly zero before its next resonance. And although the sponge exhibits a broadband absorption, it trades off poorer performance in higher frequencies as compared to the designed metamaterial absorber, against a somewhat better absorption at lower frequencies. This comparison emphasizes the fact that, in the causal inequality, low frequency behavior dominates the contribution to the sample thickness. Here, the somewhat better low frequency absorption of the MPP or sponge is at the cost of degrading the absorption over large ranges of higher frequencies. The novelty of our approach lies in making the absorption spectrum tunable, while integrating the causal optimality as part of the design.

In engineering practice, decibel (dB) is a more relevant unit. In Fig. S6 we compare the absorption by 6 cm of sponge against that by the 5.93 cm thick metamaterial, by their reflection loss characterized in decibels. It is seen from Fig. S6 that in the target frequency regime, i.e., above 800 Hz, our metamaterial absorber has an advantage of ~5 to 10 dB in reducing the reflection through absorption. To reach the same level of absorption within the target frequency range, the sponge thickness needs to be increased by a factor of at least 50%. If the thin walls can be technically realized in our metamaterial unit, then the advantage over conventional absorbers can be fairly substantial within the target range, i.e, between 10-15 dB if the solid red line is used for comparison in Fig. S6.

References

1. R. M. Fano. *J. Franklin Inst.*, 1950, **249**, 57–83.
2. K. N. Rozanov. *IEEE Trans. Antennas. Propag.*, 2000, **48**, 1230–1234.
3. M. Yang, G. Ma, Y. Wu, Z. Yang, P. Sheng. *Phys. Rev. B*, 2014, **89**, 064309.
4. D-Y. Maa. *J. Acoust. Soc. Am*, 1998, **104**, 2861–2866.
5. J. Allard and N. Atalla. *Propagation of Sound in Porous Media: Modeling Sound Absorbing Materials.* 2nd Edition (John Wiley & Sons, 2009).
6. D. L. Johnson, J. Koplik, R. Dashen. *J. Fluid Mech*, 1987, **176**, 379–402.